Electronic Supporting Information

Crystal Structure and Temperature-Dependent Luminescence of a Heterotetranuclear Sodium-Europium(III) *β*-diketonate Complex

Sofia M. Bruno,[a] Duarte Ananias,*[a] Filipe A. Almeida Paz,[a] Martyn Pillinger,[a] Anabela A. Valente,[a] Luís D. Carlos[b] and Isabel S. Gonçalves*[a]

[a] *Department of Chemistry, CICECO, University of Aveiro, Campus Universitário de Santiago, 3810-193 Aveiro, Portugal. E-mail: dananias@ua.pt (D. Ananias), igoncalves@ua.pt (I. S. Gonçalves)*

[b] *Department of Physics, CICECO, University of Aveiro, Campus Universitário de Santiago, 3810-193 Aveiro, Portugal*

General methods and materials

Microanalyses for CHN were performed at the Department of Chemistry, University of Aveiro. FT-IR spectra were obtained as KBr pellets using a FTIR Mattson-7000 spectrophotometer and recorded from 4000 to 350 cm^{-1}. Raman spectra were recorded on a Bruker RFS100/S FT spectrometer, using a Nd:YAG laser with an excitation wavelength of 1064 nm. Reagents were purchased from commercial sources and used as received. Literature procedures were used to prepare tris(3,5-dimethyl-1-pyrazolyl)methane (tpm*).[1]

The emission and excitation spectra were recorded using a Fluorolog-2® Horiba Scientific (Model FL3-2T) spectroscope, with a modular double grating excitation spectrometer (fitted with a 1200 grooves/mm grating blazed at 330 nm) and a TRIAX 320 single emission monochromator (fitted with a 1200 grooves/mm grating blazed at 500 nm, reciprocal linear density of 2.6 nm.mm^{-1}), coupled to a R928 Hamamatsu photomultiplier, using the front face acquisition mode. The excitation source was a 450 W Xe arc lamp. The emission spectra were corrected for detection and optical spectral response of the spectrofluorimeter and the excitation spectra were corrected for the spectral distribution of the lamp intensity using a photodiode reference detector. Time-resolved measurements were carried out using a 1934D3 phosphorimeter coupled to the Fluorolog®-3, and a Xe-Hg flash lamp (6 μs/pulse half width and 20-30 μs tail) was used as the excitation source. The variable temperature measurements were performed using a helium-closed cycle cryostat with vacuum system measuring ~10^{-6} mbar and a Lakeshore 330 auto-tuning temperature controller with a resistance heater. The temperatures were adjusted from *ca.*15 to 373 K.

The absolute emission quantum yields were measured at room temperature using a quantum yield measurement system C9920-02 from Hamamatsu with a 150 W Xenon lamp coupled to a monochromator for wavelength discrimination, an integrating sphere as sample chamber and a multi channel analyser for signal detection. Three measurements were made for each sample and the average value is reported. The method is accurate to within 10%.

Preparation of $[Eu_2Na_2(nta)_2(CF_3CO_2)_4(naphCO_2)_2(tpm^*)_2]\cdot H_2O$ (1)

Hnta (0.64 g, 2.40 mmol) was dissolved in ethanol (8 mL) at 50 ºC. Then, 1 M NaOH (2.4 mL) was added at ambient temperature, and after stirring for 15 min the pH was confirmed to be in the range 8-9. A solution of $EuCl_3\cdot 6H_2O$ (0.29 g, 0.80 mmol) in water (10 mL) was slowly added, and the suspension was stirred at ambient temperature for 4 h. A solution of tpm* (0.24 g, 0.80 mmol) in $CHCl_3$ (10 mL) was then added and the resultant mixture stirred for 5 h. After complete evaporation of the solvents under reduced pressure, the resultant yellow solid was washed with hexane (3×20 mL), dried under reduced pressure, and recrystallised at ambient temperature by slow diffusion of diethyl ether into a concentrated solution of the product in CH_2Cl_2/hexane. Yield (Eu basis): 0.40 g, 44%. Anal. Calcd for $C_{90}H_{74}Eu_2F_{18}N_{12}Na_2O_{16}\cdot H_2O$ (2289.52): C 47.21, H 3.35, N 7.34%. Found: C 47.45, H 3.73, N 6.84%. FT-IR (KBr, ν/cm^{-1}): 3434br, 3057m, 2979m, 2956m, 2928m, 2872w, 1692s, 1664m, 1633m, 1616s, 1593w, 1568m, 1532m, 1509m, 1472m, 1454w, 1439w, 1420s, 1386m, 1366w, 1332w, 1308m, 1288s, 1261m, 1201vs, 1143s, 1070w, 1027m, 970m, 955m, 935vw, 925vw, 916vw, 903vw, 889w, 858m, 836w, 808sh, 790s, 765m, 756w, 727m, 719m, 702m, 686m, 632w, 596m, 571m, 521m, 485m, 474m, 378m. FT-Raman (ν/cm^{-1}): 3056m, 2922m, 1633s, 1619s, 1596s, 1570m, 1530m, 1510m, 1475vs, 1433m, 1387vs, 1366vw, 1353m, 1288m, 1218m, 1199m, 1167w, 1144m, 1125m, 1038vw, 1018m, 956w, 935m, 890vw, 869vw, 850vw, 838w, 789vw, 771s, 717vw, 686vw, 628vw, 590m, 518m, 464w, 398w, 352w, 298w, 257w, 230w, 193m, 140m, 104m.

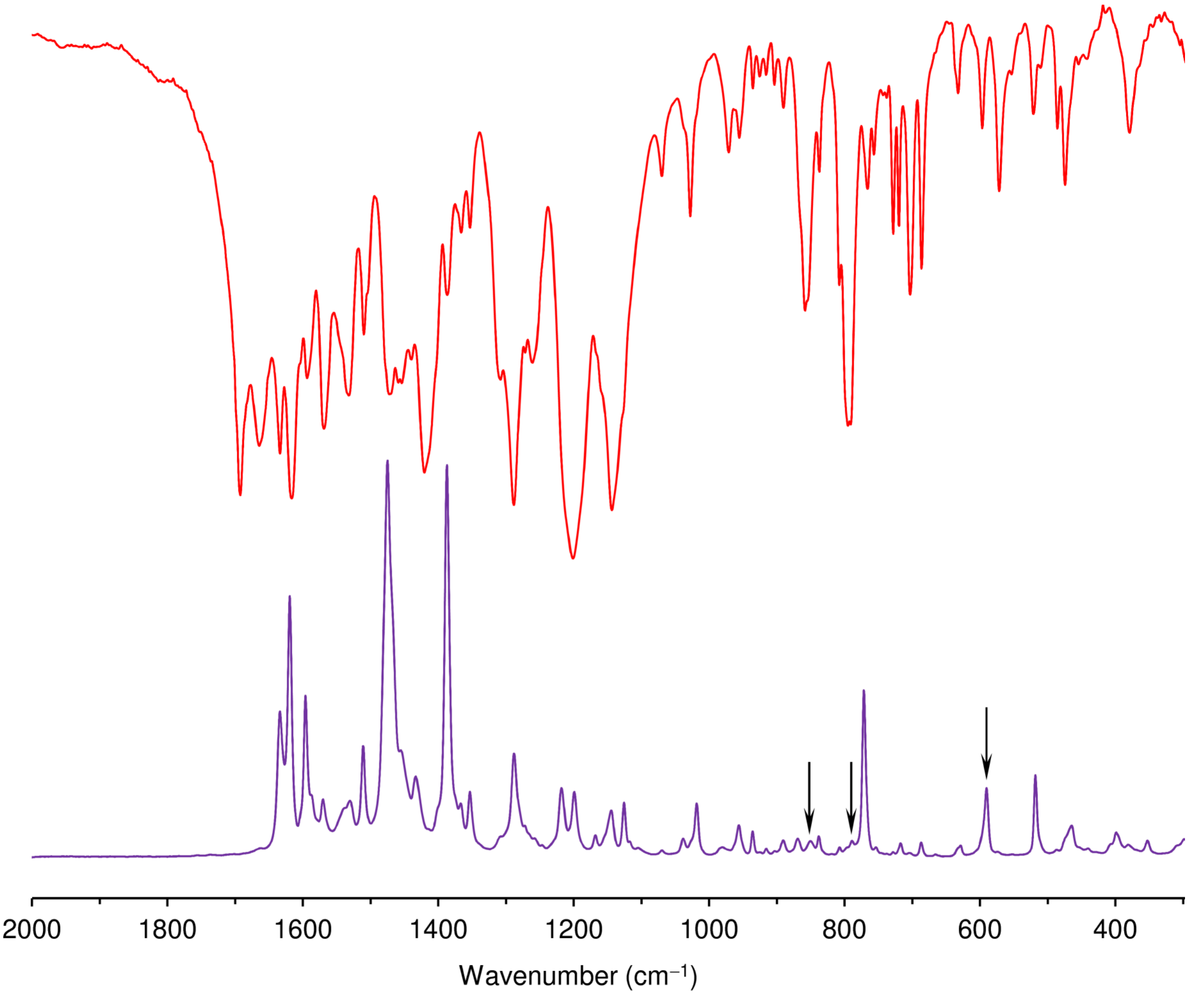

Fig. S1 FT-IR (red) and FT-Raman (violet) spectra of complex **1** in the range 300-2000 cm^{-1}. The vertical black arrows identify the Raman vibronic modes associated with faint emission lines in the emission spectrum of **1** (Fig. S6).

Single-Crystal X-ray Diffraction

Single crystals of $[Eu_2Na_2(nta)_2(CF_3CO_2)_4(naphCO_2)_2(tpm^*)_2]\cdot H_2O$ (**1**) [where nta$^-$ = 1-(2-naphthoyl)-3,3,3-trifluoroacetonate, $CF_3CO_2^-$ = trifluoroacetate, $naphCO_2^-$ = naphthalene-2-carboxylate] were manually harvested from the crystallisation vial and immersed in highly viscous FOMBLIN Y perfluoropolyether vacuum oil (LVAC 140/13, Sigma-Aldrich) to avoid degradation caused by the evaporation of the solvent.[2] Crystals were mounted on a Hampton Research CryoLoop with the help of a Stemi 2000 stereomicroscope equipped with Carl Zeiss lenses. Data were collected on a Bruker X8 Kappa APEX II CCD area-detector diffractometer (Mo-Kα graphite-monochromated radiation, λ = 0.71073 Å) controlled by the

APEX2 software package[3] and equipped with an Oxford Cryosystems Series 700 cryostream monitored remotely using the software interface Cryopad.[4] Images were processed using the software package SAINT+,[5] and data were corrected for absorption by the multiscan semi-empirical method implemented in SADABS.[6] The structure was solved using the Patterson synthesis algorithm implemented in SHELXS-2014,[7] which allowed the immediate location of the crystallographically independent metal centres and most of the heaviest atoms. The remaining non-hydrogen atoms were located from difference Fourier maps calculated from successive full-matrix least-squares refinement cycles on F^2 using the latest SHELXL from the 2014 release.[7b,8] All structural refinements were performed using the graphical interface ShelXle.[9] All non-hydrogen atoms were successfully refined using anisotropic displacement parameters.

The terminal $–CF_3$ groups from both trifluoroacetate anions were found to have rotational disorder. This disorder was included in the final structural model by assuming two distinct crystallographic positions for each group. The fluorine atoms of each disordered $–CF_3$ group were modelled using a common isotropic displacement parameter. In addition, the geometrical features of these groups were heavily restrained by using common and refineable C–F and F•••F interatomic distances for all groups, which ultimately refined to 1.326(3) and 2.113(4) Å, respectively.

The interstitial spaces between the tetranuclear $[Eu_2Na_2(nta)_2(CF_3CO_2)_4(naphCO_2)_2(tpm^*)_2]$ complexes were found to be occupied by highly disordered water molecules of crystallization. The asymmetric unit was modeled as comprised of two crystallographic positions for this chemical moiety, each with a fixed site occupancy of 0.25. Even though the hydrogen atoms could not be located from difference Fourier maps, and attempts to place these on calculated positions failed to produce stable structural refinements, these hydrogen atoms have been included in the empirical formula of the compound (Table S1). The two oxygen atoms were modeled by assuming independent isotropic displacement parameters.

Hydrogen atoms bound to carbon were placed at their idealised positions using appropriate *HFIX* instructions in SHELXL: *137* for the $–CH_3$ methyl groups, *43* for the CH groups of the aromatic rings and *13* for the tertiary carbon atom (of the tpm* chelating organic ligand). All hydrogen atoms were included in subsequent refinement cycles with isotropic thermal displacement parameters (U_{iso}) fixed at $1.2\times U_{eq}$ (CH groups) or $1.5\times U_{eq}$ (methyl groups) of the parent carbon atoms.

The last difference Fourier map synthesis showed the highest peak (1.609 e$Å^{-3}$) and the deepest hole (−1.140 e$Å^{-3}$) located at 0.70 and 0.44 Å from F4 and F5', respectively, both belonging to a disordered terminal –CF_3 group.

Information concerning crystallographic data collection and structure refinement details is summarised in Table S1. Tables S2 and S3 summarise the most relevant geometrical parameters of the two crystallographically independent metal coordination environments. Table S4 lists the most structurally relevant supramolecular contacts present in the crystal structure of complex **1**. Structural drawings have been created using the software package Crystal Impact Diamond.[10] Molecular model units and rotation movies were created using CrystalMaker.[11]

Crystallographic data (including structure factors) for the crystal structure of complex **1** have been deposited with the Cambridge Crystallographic Data Centre as supplementary publication No. CCDC-1008766. Copies of the data can be obtained free of charge via www.ccdc.cam.ac.uk/conts/retrieving.html.

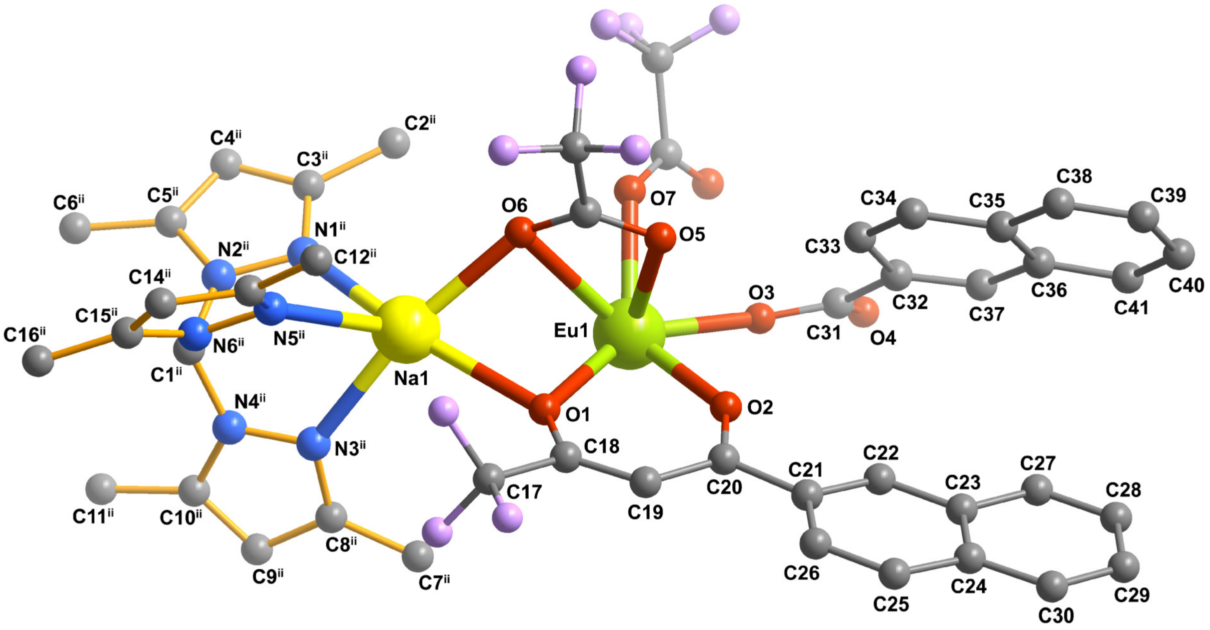

Fig. S2 Asymmetric unit of $[Eu_2Na_2(nta)_2(CF_3CO_2)_4(naphCO_2)_2(tpm^*)_2]\cdot H_2O$ (**1**) (*please note*: hydrogen atoms and the disorder of the –CF_3 moieties have been omitted for clarity), emphasising the seven distinct chemical moieties composing the tetranuclear complex. The atomic labelling for selected atoms (mainly those which can be involved in the supramolecular contacts – see Table S4) has been provided. For selected bond lengths and angles see Tables S2 and S3. Symmetry transformation used to generate equivalent atoms: (ii) -1+x, y, z. Colour scheme as in Fig. S5.

Table S1 Crystal and structure refinement data for compound $[Eu_2Na_2(nta)_2(CF_3CO_2)_4(naphCO_2)_2(tpm^*)_2]\cdot H_2O$ (**1**)

Formula	$C_{90}H_{76}Eu_2F_{18}N_{12}Na_2O_{17}$
Formula weight	2289.52
Crystal system	Monoclinic
Space group	$P2_1/n$
a/Å	15.2602(6)
b/Å	16.4953(6)
c/Å	19.5100(7)
γ/°	92.256(2)
Volume/Å^3	4907.3(3)
Z	2
D_c/g cm^{-3}	1.549
μ(Mo-Kα)/mm^{-1}	1.379
Crystal size/mm	0.20×0.20×0.12
Crystal type	Yellow blocks
θ range	3.53 to 27.48
Index ranges	$-19 \leq h \leq 19$, $-21 \leq k \leq 19$, $-25 \leq l \leq 25$
Reflections collected	89952
Independent reflections	11036 [$R_{\text{int}} = 0.0537$]
Completeness to $\theta = 25.24$°	99.3%
Final R indices [$I>2\sigma(I)$]^{a,b}	$R1 = 0.0675$, $wR2 = 0.1474$
Final R indices (all data)^{a,b}	$R1 = 0.1220$, $wR2 = 0.1777$
Weighting scheme^{c}	$m = 0.0418$, $n = 37.0594$
Largest diff. peak and hole	1.609 and −1.140 eÅ^{-3}

$^{a}R1 = \sum\left\|F_o\right|-\left|F_c\right\|/\sum\left|F_o\right|$; $^{b}wR2 = \sqrt{\sum\left[w\left(F_o^2-F_c^2\right)^2\right]/\sum\left[w\left(F_o^2\right)^2\right]}$

$^{c}w = 1/\left[\sigma^2\left(F_o^2\right)+\left(mP\right)^2+nP\right]$ where $P = \left(F_o^2+2F_c^2\right)/3$

Table S2 Bond angles (in degrees) for the two crystallographically independent metal centers present in **1**[a]

O1–Eu1–O3^{i}	120.13(16)	O3–Eu1–O6	137.32(17)
O1–Eu1–O4^{i}	75.41(16)	O3^{i}–Eu1–O6	113.74(15)
O1–Eu1–O5	84.41(19)	O3–Eu1–O7	73.45(18)
O1–Eu1–O6	66.39(17)	O3–Eu1–O8^{i}	80.17(18)
O1–Eu1–O7	135.58(19)	O4^{i}–Eu1–O3^{i}	51.19(15)
O1–Eu1–O8^{i}	80.40(18)	O4^{i}–Eu1–O5	124.77(17)
O2–Eu1–O1	73.61(17)	O4^{i}–Eu1–O6	74.22(16)
O2–Eu1–O3	78.04(16)	O5–Eu1–O3^{i}	145.33(18)
O2–Eu1–O3^{i}	133.76(17)	O5–Eu1–O6	50.64(16)
O2–Eu1–O4^{i}	141.80(17)	O7–Eu1–O3^{i}	71.51(17)
O2–Eu1–O5	73.58(19)	O7–Eu1–O4^{i}	85.82(18)
O2–Eu1–O6	112.05(16)	O7–Eu1–O5	73.9(2)
O2–Eu1–O7	132.27(18)	O7–Eu1–O6	69.88(17)
O2–Eu1–O8^{i}	72.39(17)	O8^{i}–Eu1–O3^{i}	67.77(16)
O3–Eu1–O1	149.36(17)	O8^{i}–Eu1–O4^{i}	80.93(17)
O3–Eu1–O3^{i}	73.01(17)	O8^{i}–Eu1–O5	145.42(17)
O3–Eu1–O4^{i}	124.15(16)	O8^{i}–Eu1–O6	142.38(17)
O3–Eu1–O5	98.64(18)	O8^{i}–Eu1–O7	136.33(17)
O4^{i}–Na1–O1	72.32(18)	O6–Na1–N5^{ii}	116.0(2)
O4^{i}–Na1–O6	81.00(19)	N1^{ii}–Na1–O1	157.1(2)
O4^{i}–Na1–N1^{ii}	84.8(2)	N1^{ii}–Na1–N5^{ii}	73.4(2)
O4^{i}–Na1–N3^{ii}	86.6(2)	N3^{ii}–Na1–O1	103.1(2)
O4^{i}–Na1–N5^{ii}	155.4(2)	N3^{ii}–Na1–N1^{ii}	76.5(2)
O6–Na1–O1	68.31(18)	N3^{ii}–Na1–N5^{ii}	77.4(2)
O6–Na1–N1^{ii}	107.2(2)	N5^{ii}–Na1–O1	129.3(2)
O6–Na1–N3^{ii}	166.6(2)		

[a] Symmetry transformations used to generate equivalent atoms: (i) -*x*, -*y*, 1-*z*; (ii) -1+*x*, *y*, *z*.

Table S3 Bond distances (in Å) for the two crystallographically independent metal centers present in **1**^{a}

Eu1–O1	2.370(5)	Na1–O1	2.578(6)
Eu1–O2	2.342(5)	Na1–O4^{i}	2.396(6)
Eu1–O3	2.349(5)	Na1–O6	2.397(6)
Eu1–O3^{i}	2.584(5)	Na1–N1^{ii}	2.468(7)
Eu1–O4^{i}	2.434(5)	Na1–N3^{ii}	2.442(7)
Eu1–O5	2.457(5)	Na1–N5^{ii}	2.492(7)
Eu1–O6	2.712(5)		
Eu1–O7	2.410(5)		
Eu1–O8^{i}	2.408(5)		

^{a} Symmetry transformations used to generate equivalent atoms: (i) -*x*, -*y*, 1-*z*; (ii) -1+*x*, *y*, *z*.

Table S4 Geometrical details (distances in Å and angles in degrees) of the weak hydrogen bonds and intermolecular close contacts present in **1**^{a,b}

D–H···A	***d*(D···A)**	**<(DHA)**
C1–H6B···F7^{iii}	3.465(13)	162
C11–H11A···F9’^{iv}	3.380(16)	152
C12–H12A···F8^{v}	3.352(12)	132
C12–H12B···F5^{vi}	3.402(12)	145
C16–H16C···F4^{iii}	3.300(14)	136
C37–H37···N1^{vii}	3.437(10)	163
π-π Contacts	***Inter-centroid distance***	
*Cg*1···*Cg*1^{vii}	3.631(5)	
C–H···*Cg*	***d*(C···*Cg*)**	**<(CH*Cg*)**
C2–H2C···*Cg*2^{iii}	3.713(10)	132
C16–H16B···*Cg*3^{viii}	3.776(12)	140

^{a} Symmetry transformations used to generate equivalent atoms: (iii) ½+*x*, ½-*y*, -½+*z*; (iv) ½-*x*, -½+*y*, ½-*z*; (v) 1.5+*x*, ½-*y*, -½+*z*; (vi) 1+*x*, *y*, *z*; (vii) 1-*x*, -*y*, 1-*z*; (viii) 2-*x*, -*y*, -*z*.

^{b} Centres of gravity (*C*g) (see Fig. S2): *C*g1 = C21, C22, C23, C24, C25 and C26; *C*g2 = C35, C36, C38, C39, C40 and C41; *C*g3 = N3, N4, C8, C9 and C10.

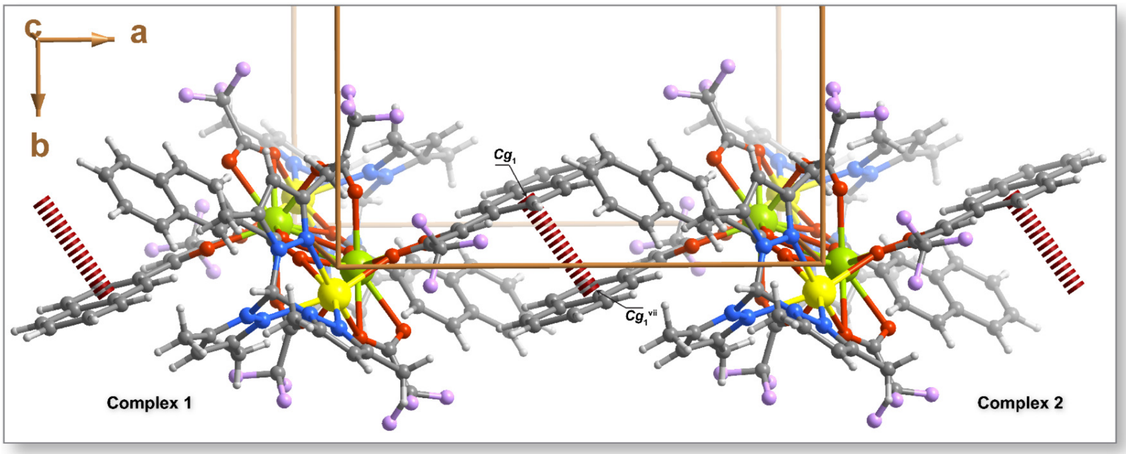

Fig. S3 Schematic representation of the chain of π-π supramolecular contacts (Table S4) running parallel to the *a*-axis of the unit cell, promoting the interconnection of adjacent tetranuclear complexes *via* the chelated nta⁻ moieties. Colour scheme as in Fig. S5.

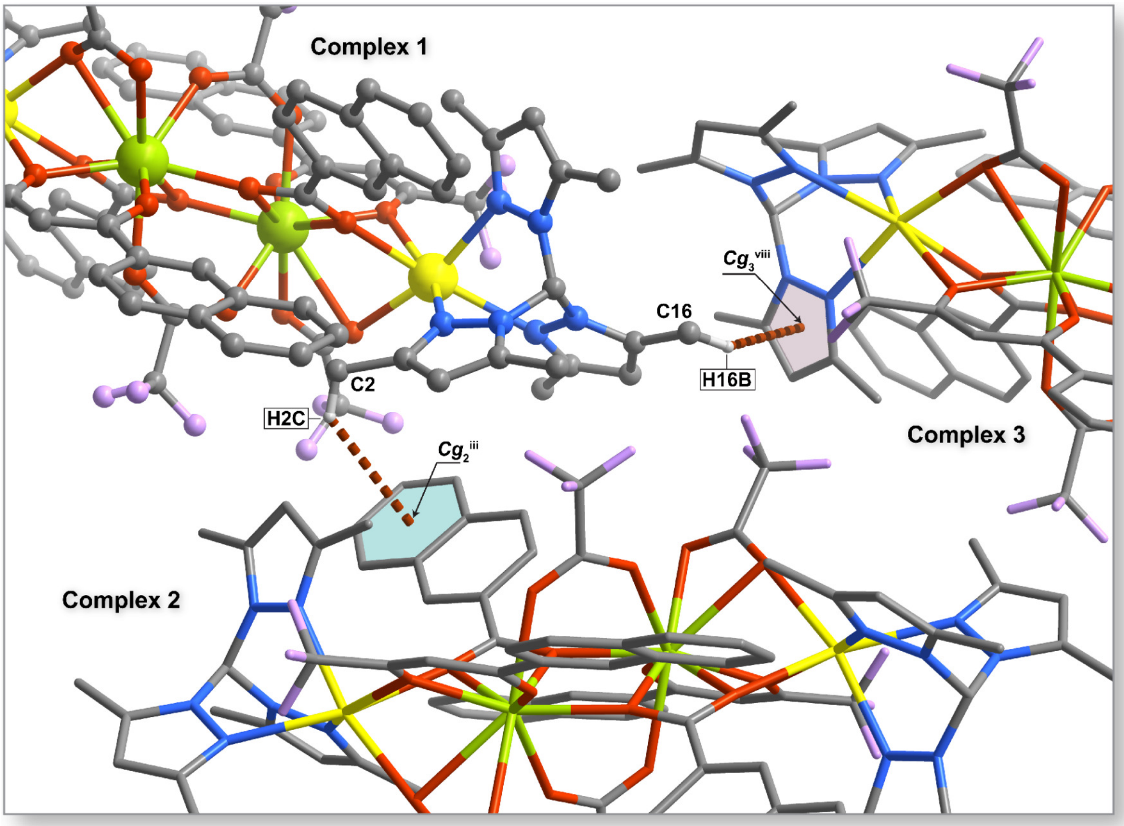

Fig. S4 Schematic representation of the weak C–H···*Cg* supramolecular contacts (Table S4) present in the crystal structure of **1**. Colour scheme as in Fig. S5.

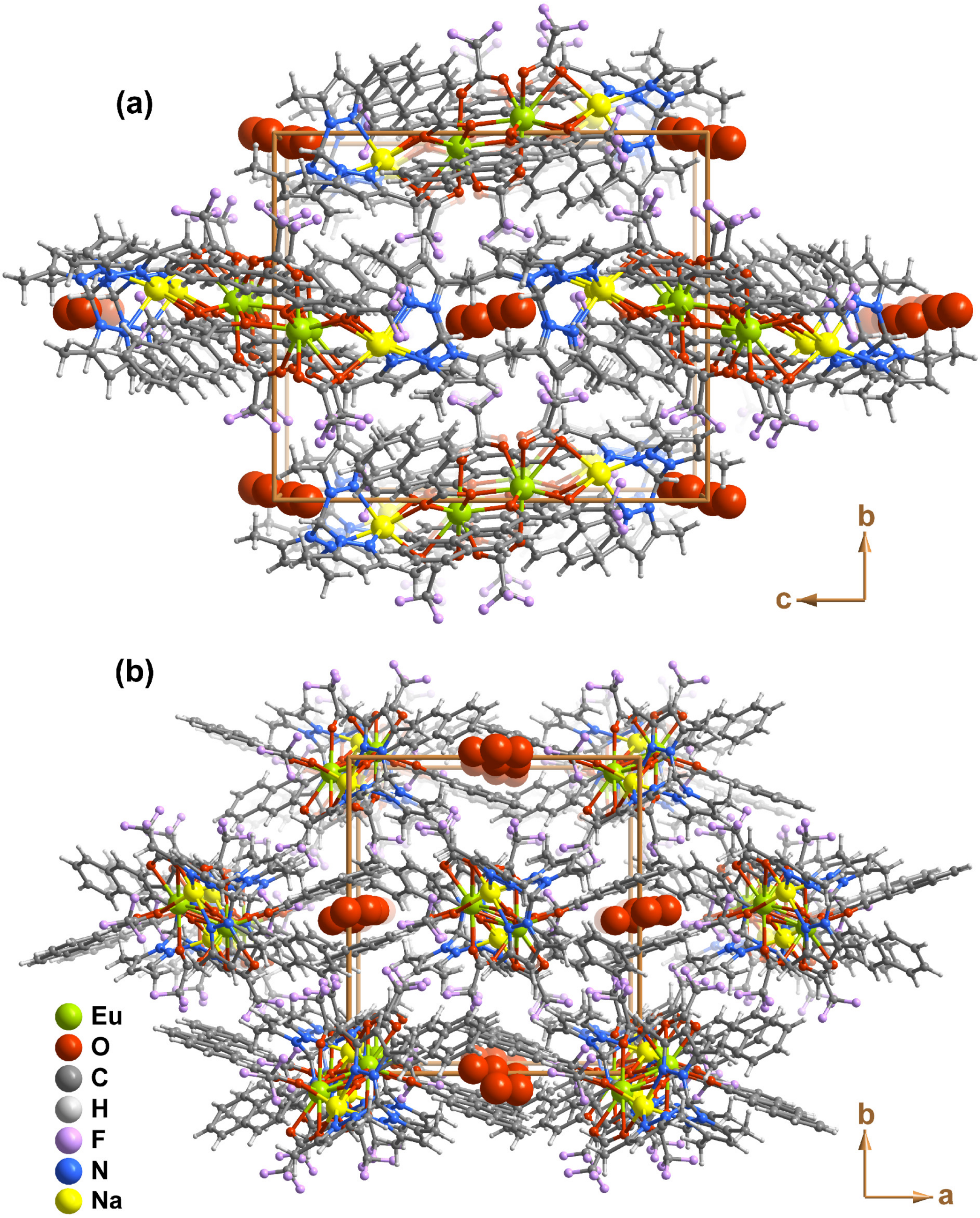

Fig. S5 Schematic representations of the crystal packing of $[Eu_2Na_2(nta)_2(CF_3CO_2)_4(naphCO_2)_2(tpm^*)_2]\cdot H_2O$ (**1**) viewed in perspective along the (a) [100] and (b) [001] directions of the unit cell. The disordered water molecules of crystallisation are represented in space-filling mode.

Photoluminescence spectroscopy

Based on the emission spectra, $^5D_0$ lifetimes and empirical radiative and non-radiative transition rates, the $^5D_0$ quantum efficiency, q, has been determined for complex **1.**[12-14] Assuming that only non-radiative and radiative processes are involved in the depopulation of the $^5D_0$ state, q is given by:

$$q = \frac{k_r}{k_r + k_{nr}} \quad (1)$$

where k_r and k_{nr} are the radiative and non-radiative transition probabilities, respectively, and $k_{exp}=\tau_{exp}^{-1}$ $(k_r + k_{nr})$ is the experimental transition probability. The emission intensity, I, taken as the integrated intensity S of the emission lines for the $^5D_0 \rightarrow {}^7F_{0-6}$ transitions, is given by:

$$I_{i \rightarrow j} = \hbar w_{i \rightarrow j} A_{i \rightarrow j} N_i \equiv S_{i \rightarrow j} \quad (2)$$

where i and j represent the initial ($^5D_0$) and final ($^7F_{0-6}$) levels, respectively, $\hbar w_{i \rightarrow j}$ is the transition energy, $A_{i \rightarrow j}$ is the Einstein coefficient of spontaneous emission and N_i is the population of the $^5D_0$ emitting level.[12-14] Because the $^5D_0 \rightarrow {}^7F_{5,6}$ transitions are not observed experimentally, their influence on the depopulation of the $^5D_0$ excited state may be neglected and, thus, the radiative contribution is estimated based only on the relative intensities of the $^5D_0 \rightarrow {}^7F_{0-4}$ transitions. The emission integrated intensity, S, of the $^5D_0 \rightarrow {}^7F_{0-4}$ transitions has been measured for sample **1** at 296 K.

Because the $^5D_0 \rightarrow {}^7F_1$ transition does not depend on the local ligand field seen by the Eu^{3+} ions (due to its dipolar magnetic nature) it may be used as a reference for the whole spectrum, *in vacuo* $A(^5D_0 \rightarrow {}^7F_1)=14.65$ s^{-1},[15] and k_r is given by:

$$k_r = A_{0 \rightarrow 1} \frac{\hbar \omega_{0 \rightarrow 1}}{S_{0 \rightarrow 1}} \sum_{J=0}^{4} \frac{S_{0-J}}{\hbar \omega_{0-J}} \quad (3)$$

where A_{0-1} is the Einstein coefficient of spontaneous emission between the $^5D_0$ and the $^7F_1$ levels. An average index of refraction of 1.5 was considered for the sample, leading to $A(^5D_0 \rightarrow {}^7F_1) \approx 50$ s^{-1} .[16]

Table S5 Experimental $^5D_0$ lifetime (τ), radiative (k_r) and non-radiative (k_{nr}) transition rates, $^5D_0$ quantum efficiency (q), and the absolute emission quantum yield (η, for 370 nm excitation wavelength) for **1**

Temperature	τ [ms]	k_r [s^{-1}]	k_{nr} [s^{-1}]	q [%]	η [%]
296 K	0.68±0.01	857	616	58	39

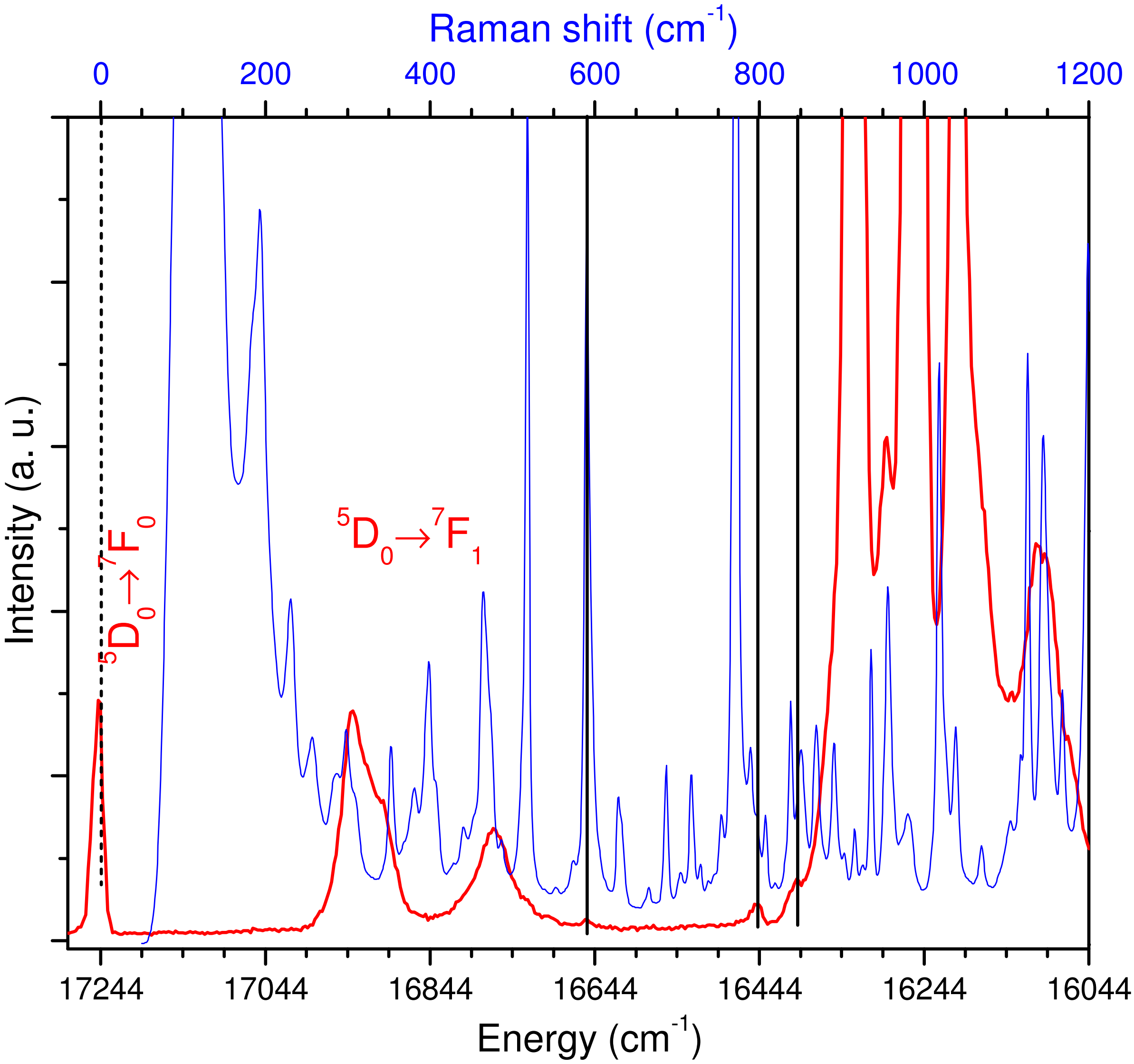

Fig. S6 Emission spectrum of **1** (15 K, excitation wavelength of 370 nm) magnified in the $^5D_0 \rightarrow {}^7F_{1\text{-}2}$ region (red line) and corresponding vibrational Raman spectrum recorded at ambient temperature (blue line). The vertical black lines identify the faint emission lines associated with the Raman vibronic modes.

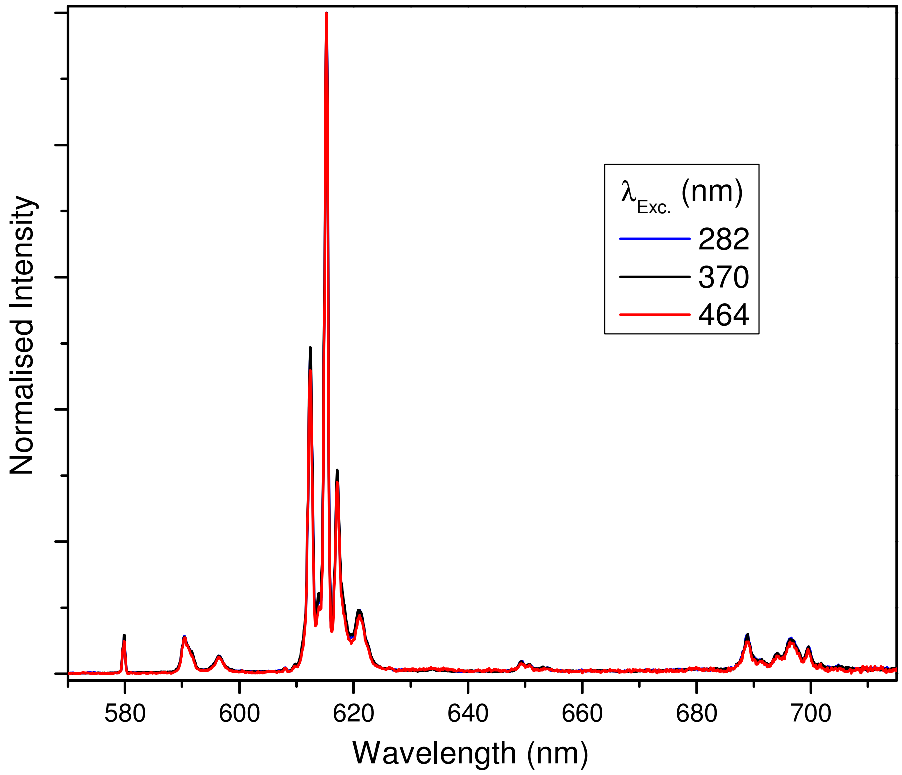

Fig. S7 Emission spectra of **1** recorded at 15 K with distinct excitation wavelengths.

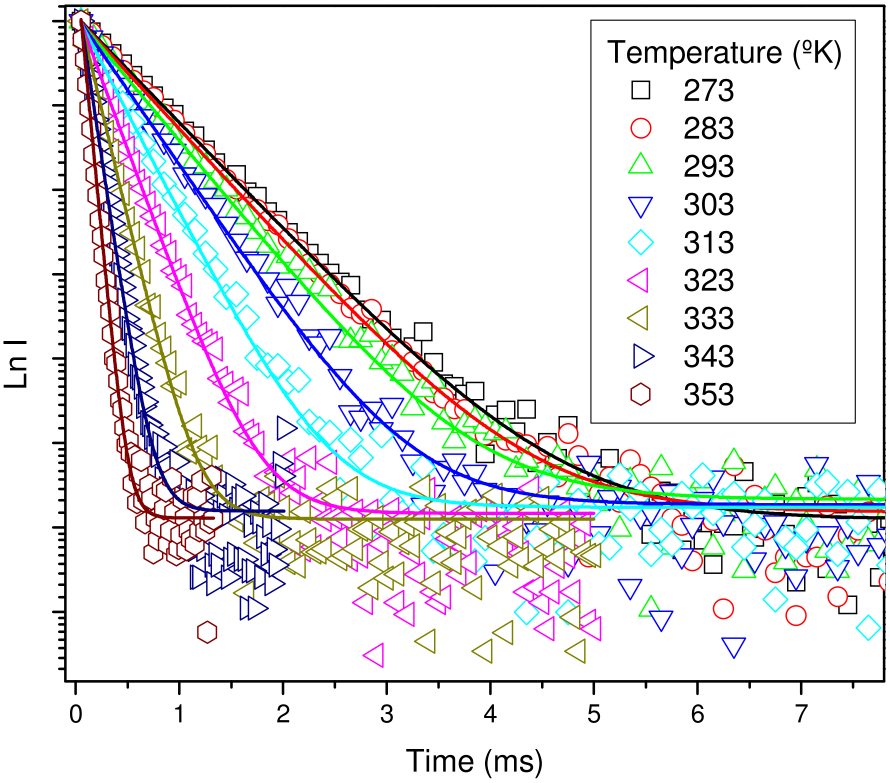

Fig. S8 $^5D_0$ decay curves with corresponding fits using exponential decay functions. The emission was monitored at 615 nm and the excitation fixed at 370 nm.

Table S6 Lifetime values of **1** monitoring the emission at 612 nm, under 370 nm excitation. All decay curves have been fitted with a single exponential function with r^2 values better than 0.999

Temperature (K)	**Lifetime (ms)**	**Fitting error (ms)**
14	0.816	0.004
50	0812	0.004
100	0.824	0.002
150	0.830	0.003
200	0.814	0.005
250	0.804	0.004
263	0.796	0.004
273	0.787	0.003
283	0.746	0.005
293	0.672	0.004
303	0.558	0.003
313	0.419	0.002
323	0.297	0.002
333	0.191	0.003
343	0.122	0.002
353	0.077	0.001
363	0.058	0.001

References

1. P. Neves, S. Gago, S. S. Balula, A. D. Lopes, A. A. Valente, L. Cunha-Silva, F. A. A. Paz, M. Pillinger, J. Rocha, C. M. Silva and I. S. Gonçalves, *Inorg. Chem.* 2011, **50**, 3490–3500.
2. T. Kottke and D. Stalke, *J. Appl. Crystallogr.*, 1993, **26**, 615-619.
3. APEX2, *Data Collection Software, Version 2.1-RC13*, Bruker AXS, Delft, The Netherlands, 2006.

4. Cryopad, *Remote monitoring and control, Version 1.451*, Oxford Cryosystems, Oxford, United Kingdom, 2006.
5. SAINT+, *Data Integration Engine, Version 8.27b*©, 1997-2012, Bruker AXS, Madison, Wisconsin, USA.
6. G. M. Sheldrick, *SADABS 2012/1*, Bruker AXS Area Detector Scaling and Absorption Correction 2012, Bruker AXS, Madison, Wisconsin, USA.
7. (a) G. M. Sheldrick, *SHELXS-2014, Program for Crystal Structure Solution*, University of Göttingen, 2014; (b) G. M. Sheldrick, *Acta Cryst. A*, 2008, **64**, 112-122.
8. G. M. Sheldrick, *SHELXL, Version 2014/3*, Program for Crystal Structure Refinement, University of Göttingen, 2014.
9. C. B. Hübschle, G. M. Sheldrick and B. Dittric, *J. Appl. Crystallogr.*, 2011, **44**, 1281-1284.
10. K. Brandenburg, *DIAMOND, Version 3.2f*, Crystal Impact GbR, Bonn, Germany, 1997-2010.
11. CrystalMaker®, *Version 9.0.1*, 1994-2014, CrystalMaker Software Ltd.
12. L. D. Carlos, Y. Messaddeq, H. F. Brito, R. A. Sá Ferreira, V. De Zea Bermudez and S. J. L. Ribeiro, *Adv. Mater.*, 2000, **12**, 594-598.
13. O. L. Malta, H. F. Brito, J. F. S. Menezes, F. R. Gonçalves e Silva, S. Alves Jr., F. S. Farias Jr. and A. V. M. de Andrade, *J. Lumin.*, 1997, **75**, 255-268.
14. O. L. Malta, M. A. Couto dos Santos, L. C. Thompson and N. K. Ito, *J. Lumin.*, 1996, **69**, 77-84.
15. M. H. V. Werts, R. T. F. Jukes and J. W. Verhoeven, *Phys. Chem. Chem. Phys.*, 2002, **4**, 1542-1548.
16. M. F. Hazenkamp and G. Blasse, *Chem. Mater.*, 1990, **2**, 105-110.